Atom Transfer Radical Polymerization from Nanoparticles: A Tool for the Preparation of Well-Defined Hybrid Nanostructures and for Understanding the Chemistry of Controlled/"Living" Radical Polymerizations from Surfaces

Timothy von Werne and Timothy E. Patten*

Contribution from the Department of Chemistry, University of California at Davis, One Shields Avenue, Davis, California 95616-5295

Received January 26, 2001

Abstract: Structurally well-defined polymer−nanoparticle hybrids were prepared by modifying the surface of silica nanoparticles with initiators for atom transfer radical polymerization and by using these initiator-modified nanoparticles as macroinitiators. Well-defined polymer chains were grown from the nanoparticle surfaces to yield individual particles composed of a silica core and a well-defined, densely grafted outer polystyrene or poly(methyl methacrylate) layer. In both cases, linear kinetic plots, linear plots of molecular weight (M_n) versus conversion, increases in hydrodynamic diameter with increasing conversion, and narrow molecular weight distributions (M_w/M_n) for the grafted polymer samples were observed. Polymerizations of styrene from smaller (75-nm-diameter) silica nanoparticles exhibited good molecular weight control, while polymerizations of methyl methacrylate (MMA) from the same nanoparticles exhibited good molecular weight control only when a small amount of free initiator was added to the polymerization solution. The difference in polymerization behavior for styrene and MMA was ascribed to the facts that styrene undergoes thermal self-initiation while MMA does not and that termination processes involving freely diffusing chains are faster than those involving surface-bound chains. The polymerizations of both styrene and MMA from larger (300-nm-diameter) silica nanoparticles did not exhibit molecular weight control. This lack of control was ascribed to the very high initial monomer-to-initiator ratio in these polymerizations. Molecular weight control was induced by the addition of a small amount of free initiator to the polymerization but was not induced when 5−15 mol % of deactivator (Cu(II) complex) was added.

Introduction

The optical and magnetic properties of nanoparticles have been well documented. In order to take advantage of these properties on the macroscopic scale, the particles must be incorporated into a host material possessing desirable properties, such as good processing characteristics, charge carrier mobility, or transparency. In the case of polymer/nanoparticle composite materials, optimum control over the structure of the composite could be achieved by preassembling the inorganic nanoparticles with the organic polymer. One could specify the exact structure of each of the components comprising the final material, and the material could be cast into films or molded. Known methods for grafting polymer chains to particle surfaces entail chemisorption of a reactive polymer end group to the surface,[1−3] grafting a polymer chain through a monomer covalently linked to the surface,[4−7] or grafting a polymer chain from a surface modified with polymerization initiators.[8−10] Of these methods, maximum structural control can be achieved by the "grafting from" route.

For the grafting process, a controlled/"living" polymerization technique would be optimal, because such methods afford control over the molecular weight, molecular weight distribution, and structure of the resulting polymer.[11] The application of controlled/"living" polymerizations to nanocomposite synthesis is relatively unexplored. Several studies reported methods for conducting controlled/ "living" graft polymerizations from flat silicon and silica surfaces and assessed the polymerization chemistry of these surface-initiated polymerizations.[12−21] For the atom transfer radical polymerization (ATRP) systems in particular, standard conditions proved insufficient for a con-

* Corresponding author: (phone) (530) 754-6181; (fax) (530) 752-8995; (e-mail) patten@indigo.ucdavis.edu.

(1) Bridger, K.; Fairhurst, D.; Vincent, B. *J. Colloid Interface Sci.* **1979**, *68*, 190−195.
(2) Bridger, K.; Vincent, B. *Eur. Polym. J.* **1980**, *16*, 1017−1021.
(3) Auroy, P.; Auvray, L.; Leger, L. *J. Colloid Interface Sci.* **1992**, *150*, 187−194.
(4) Espiard, P.; Guyot, A. *Polymer* **1995**, *36*, 4391−4395.
(5) Jethmalani, J. M.; Ford, W. T. *Chem. Mater.* **1996**, *8*, 2138−2146.
(6) Bourgeat-Lami, E.; Lang, J. *J. Colloid Interface Sci.* **1998**, *197*, 293−308.
(7) Buchmeiser, M. R.; Sinner, F.; Mupa, M.; Wurst, K. *Macromolecules* **2000**, *33*, 32−39.
(8) Tsubokawa, N.; Kogure, A.; Maruyama, K.; Sone, Y.; Shimomura, M. *Polym. J.* **1990**, *22*, 827−833.
(9) Prucker, O.; Ruhe, J. *Macromolecules* **1998**, *31*, 602−613.
(10) Prucker, O.; Ruhe, J. *Macromolecules* **1998**, *31*, 592−601.
(11) Webster, O. W. *Science* **1991**, *251*, 887−893.
(12) Ejaz, M.; Yamamoto, S.; Ohno, K.; Tsujii, Y.; Fukuda, T. *Macromolecules* **1998**, *31*, 5934−5936.
(13) Huang, X.; Doneski, L. J.; Wirth, M. J. *Anal. Chem.* **1998**, *70*, 4023−4029.
(14) Huang, X.; Wirth, M. J. *Macromolecules* **1999**, *32*, 1694−1696.
(15) Husseman, M.; Malmstrom, E. E.; McNamara, M.; Mate, M.; Mecerreyes, D.; Benoit, D. G.; L., H. J.; Mansky, P.; Huang, E.; Russell, T. P.; Hawker, C. J. *Macromolecules* **1999**, *32*, 1424−1431.
(16) Zhao, B.; Brittain, W. J. *J. Am. Chem. Soc.* **1999**, *121*, 3557−3558.
(17) Weck, M.; Jackiw, J. J.; Rossi, R. R.; Weiss, P. S.; Grubbs, R. H. *J. Am. Chem. Soc.* **1999**, *121*, 4088−4089.

10.1021/ja010235q CCC: $20.00
Published on Web 07/17/2001

Scheme 1. Synthetic Steps for Forming Hybrid Polymer−inorganic Nanoparticles

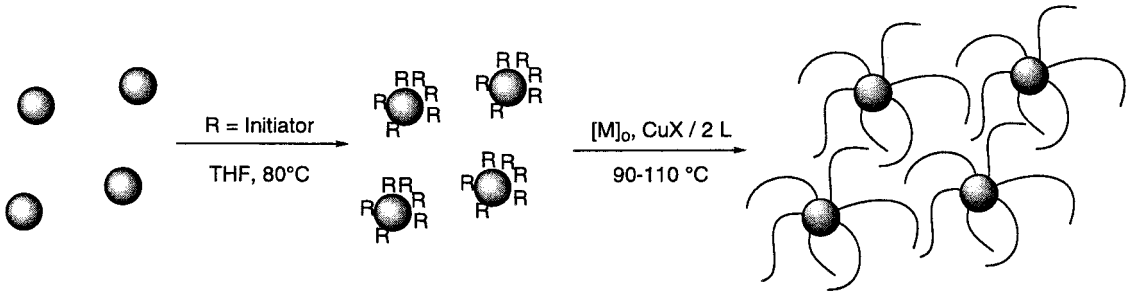

trolled polymerization from flat surfaces.[15,18] The lack of molecular weight control was manifested as a large jump in film thickness at short polymerization times and was a consequence of the low concentration of initiator in the system. The addition of deactivator[18] and the addition of "sacrificial" free initiator[15] to the polymerization system were two methods examined for inducing molecular weight control. The addition of free initiator to the polymerization medium served to lower the initial monomer-to-initiator ratio and to increase the overall initiator concentration, thereby allowing some radical coupling in solution to build up the concentration of deactivator. The addition of the $CuBr_2$/2 equiv of ligand complex in copper(I)-catalyzed ATRP systems mitigated the insufficient formation of deactivator from the small initial concentrations of initiator and copper(I) catalyst. Both studies showed that it was possible to use controlled/"living" radical polymerizations to prepare a thin film of well-defined polymer chains covalently anchored to an inorganic surface.

The chemistry of grafting polymers to and from the surfaces of nanoparticles is also a relatively new area. Gold nanoparticles were coated with alkanethiol-containing initiators for ROMP[22] and isocyanate[23] polymerizations and used to initiate living polymerizations. Latexes functionalized with initiators for ATRP were used as initiators for the polymerization of water-soluble acrylates and methacrylates.[24] Silica and silver nanoparticles have been coated with polymer using emulsion polymerizations,[25] and composite materials of silica colloidal crystals and polymer have been prepared by in situ polymerizations.[26] Also, various polymers have been attached to silica[1,2] and CdS[27] nanoparticle surfaces by chemisorption of reactive polymer chain ends.

Recently we reported a technique for conducting controlled/"living" radical polymerizations from the surface of silica nanoparticles using ATRP.[28] We found that the polymerization of styrene from the surface of 75-nm silica particles exhibited the diagnostic criteria for a controlled/"living" polymerization: an increase in the molecular weight of the pendant polymer chains with monomer conversion and a narrow molecular weight distribution for the grafted chains. In this report, we elucidate the chemistry of these grafting reactions and how changes in monomer type and particle size affect the polymerization kinetics and molecular weight control. The data are examined in the context of other ATRP studies from low surface area substrates.

Results and Discussion

To study the grafting of polymer chains from inorganic nanoparticles, we broke the problem down into two steps (Scheme 1): (1) depositing a monolayer of polymerization initiators on a nanoparticle surface and (2) conducting polymerizations using the nanoparticle as a macroinitiator and examining the effect of varying synthetic parameters, such as monomer type and nanoparticle diameter, upon the polymerization reaction. For this research, silica (SiO_2) nanoparticles were employed, because their preparation and surface chemistry are well-understood. Spherical silica particles were prepared using the Stöber process:[29,30] the hydrolysis and condensation of tetraethoxysilane in an ammonia/ethanol solution. This synthesis yields a high volume fraction of silica particles with a uniform size distribution, and the size of the particles can be controlled through variations in the initial concentrations of reagents. Accessible surface silanol groups can be derivatized using organosiloxanes, providing a means for covalent attachment of polymerization initiators to the nanoparticle surface. Among various polymerization methods, we chose to use ATRP, in particular, because it affords the molecular weight control of a living polymerization method, can be used to polymerize a range of vinyl monomers, does not require stringent conditions, and is tolerant of functional groups and impurities that are detrimental to living anionic, cationic and some transition-metal-mediated polymerizations.[31]

Tandem ATRP initiators/organosiloxanes were prepared via the hydrosilation of allyl ester group-containing ATRP initiators with dimethylethoxysilane. The use of a monosiloxane group provided a site for single attachment to the nanoparticle surface, as opposed to di-and trisiloxanes, which can form complex

(18) Matyjaszewski, K.; Miller, P.; Shukla, N.; Immaraporn, B.; Gelman, A.; Luokala, B.; Siclovan, T.; Kickelbick, G.; Vallant, T.; Hoffmann, H.; Pakula, T. *Macromolecules* **1999**, *32*, 8716−8724.

(19) Ma, H.; Davis, R. H.; Bowman, C. N. *Macromolecules* **2000**, *33*, 331−335.

(20) de Boer, B.; Simon, H. K.; Werts, M. P. L.; van der Vegte, E. W.; Hadziioannou, G. *Macromolecules* **2000**, *33*, 349−356.

(21) Kim, N. Y.; Jeon, N. L.; Choi, I. S.; Takami, S.; Harada, Y.; Finnie, K. R.; Girolami, G. S.; Nuzzo, R. G.; Whitesides, G. M.; Labinis, P. E. *Macromolecules* **2000**, *33*, 2793−2795.

(22) Watson, K. J.; Zhu, J.; Nguyen, S. T.; Mirkin, C. A. *J. Am. Chem. Soc.* **1999**, *121*, 462−463.

(23) Huber, D. L.; Carlson, G.; Gonsalves, K.; Seery, T. A. P. The Formation of Polymer Monolayers: From Adsorption to Surface Initiated Polymerizations. In *Interfacial Aspects of Multicomponent Polymer Materials*; Lohse, D. J., Russell, T. P., Sperling, L. H., Eds.; Plenum Press: New York, 1997; pp 107−122.

(24) Guerrini, M. M.; Charleux, B.; Vairon, J.-P. *Macromol. Rapid Commun.* **2000**, *21*, 669−674.

(25) Quaroni, L.; Chumanov, G. *J. Am. Chem. Soc.* **2000**, *122*.

(26) Jethmalani, J. M.; Sunkara, H. B.; Ford, W. T.; Willoughby, S. L.; Ackerson, B. J. *Langmuir* **1997**, *13*, 2633−2639.

(27) Carrot, G.; Scholz, S. M.; Plummer, C.; Hilborn, J.; Hedrick, J. *Chem. Mater.* **1999**, *11*, 3571−3577.

(28) von Werne, T.; Patten, T. E. *J. Am. Chem. Soc.* **1999**, *121*, 7409−7410.

(29) Philipse, A. P.; Vrij, A. J. *J. Colloid Interface Sci.* **1989**, *128*, 121−136.

(30) Bogush, G. H.; Tracy, M. A.; Zukowski, C. F., IV. *J. Noncryst. Solids* **1988**, *104*, 95−106.

(31) Patten, T. E.; Matyjaszewski, K. *Adv. Mater.* **1998**, *10*, 1−15.

BPDS **BIDS**

Figure 1. Structures of the monosiloxane ATRP initiators used in this study.

polymeric surface layers.[32] Two initiators were prepared for this study (Figure 1): (3-(2-bromopropionyl)propyl)dimethylethoxysilane (BPDS), in which the secondary α-bromoester could function as a styrene or acrylate ATRP initiator, and (3-(2-bromoisobutyryl)propyl)dimethylethoxysilane (BIDS), in which the tertiary α-bromoester could serve as a methacrylate ATRP initiator.

Two sets of silica particles were used in this study, 75- and 300-nm-diameter particles, that had different surface area-to-volume ratios (0.08 vs 0.02, respectively). A monolayer of the ATRP initiator was deposited on the silica nanoparticle surface by heating the siloxane initiator and nanoparticles in THF. Unreacted or dimerized initiator was washed from the particles by repeated suspension, centrifugation, and decanting of the supernatant. TEM micrographs (Figure 2) and dynamic light-scattering (DLS) analysis showed that the spherical particles remained unaggregated after surface modification. The average diameter of the particles increased slightly relative to the starting silica nanoparticles; however, this increase was within the error of the measurement. Diffuse reflectance infrared Fourier transform (DRIFT) spectroscopy was used to observe the characteristic peaks for the initiator bound to the silica surface. For example, in the DRIFT spectrum of the 75-nm-diameter BPDS-modified silica nanoparticles, a C−H stretch was visible at 2955 cm^{-1} and a C═O stretch was observed at 1738 cm^{-1}, and both of these signals were not present in spectra of the unmodified nanoparticles. The Si−O stretch due to bulk silica at 1050 cm^{-1} remained a prominent feature in the spectrum. Solid-state ^{29}Si CP-MAS NMR spectroscopy was also used to detect the presence of the surface-bound initiator on the 75-nm BPDS-modified silica nanoparticles (Figure 3). In the spectrum the chemical shifts of the Q^2, Q^3, and Q^4 silicon nuclei of bulk silica were observed as a trimodal signal at −110.8, −101.6, and −93.2 ppm, respectively. Most of the trimodal signal was composed of the Q^3 and Q^4 resonances, even though the CP-MAS technique is selective for Q^2 and Q^3 nuclei. A peak at 12.2 ppm was assigned to the resonance of the silicon nucleus of the surface-bound initiator. An approximate concentration of the surface-bound initiator in the sample was calculated by integrating the signals in a DP-MAS spectrum. The concentrations determined in this fashion were on the same order as those determined using elemental analysis. When the particle size was increased to 300 nm, the surface area-to-volume ratio decreased to a point where the amount of silane on the surface was no longer detectable using ^{29}Si NMR spectroscopy.

Elemental analysis for bromine content was used to provide a more quantitative determination of the amount of initiator on the surface of the nanoparticles. Shown in Table 1 are the initiator contents for the samples used in this study. These numbers translated into grafting densities of approximately 2−5 initiators/nm^2, which can be compared to the generally accepted surface hydroxyl content of silica of 5 OH/nm^2. Because these siloxanes should take up more volume per unit area than a hydroxyl group, the experimentally determined grafting densities indicate monolayer or near-monolayer coverages of the nanoparticle surfaces.

Both the 75- and 300-nm initiator-modified silica nanoparticles were used in standard polymerizations of styrene and methyl methacrylate (MMA). Typically, the initiator-functionalized silica was heated with monomer, copper(I) bromide, ligand, and solvent, and conversion was monitored against an internal standard using GC. Polymerization conversions were kept below 50% in order to conduct the polymerizations during the steepest part of the kinetic curve and thereby minimize the effect of the small amount of termination that is unavoidable in controlled/"living" radical polymerizations. Information about the molecular weights and molecular weight distributions of the grafted polymer was gained by etching the silica cores. Aqueous HF (5%) and a phase transfer catalyst were stirred with a toluene suspension of the polymer/silica nanoparticles. The polymer, free from silica, could then be isolated by precipitation and analyzed using GPC. In the case of etching poly(methyl methacrylate) (PMMA) grafted silica, the reaction was monitored using IR spectroscopy in order to gauge when the silica had been etched completely and to determine that no hydrolysis of the methyl ester side chains had occurred. The etching reactions typically were complete within 1−2 h at room temperature.

Shown in Figures 4−12 are the results of the polymerizations, which can be categorized into sets for 75-nm-diameter particles (Figures 4, 6, and 8) and 300-nm-diameter particles (Figures 9−12). The styrene ATRP from the 75-nm-diameter particles exhibited the characteristics of a controlled/"living" polymerization. The kinetic plot shown in Figure 5 was linear, and the plot of number-averaged molecular weight versus conversion was also linear. Each polymer sample comprising the data points had a narrow molecular weight distribution ($M_w/M_n < 1.25$). The experimental molecular weights were a factor of ∼4 higher than would be expected based upon the polymerization conversion factored with the ratio of monomer to nanoparticle initiator content. One possible explanation for this difference is that not all of the initiator sites on the nanoparticle surface initiated the growth of polymer chains, and this rationalization is consistent with the growing chains sterically blocking access of the catalyst to the neighboring initiation sites on the nanoparticle surface.

DLS measurements of the hybrid nanoparticles showed the existence of discreet particles. The hydrodynamic diameter of the composite nanoparticle also increased with the molecular weight of the pendant polymer (Table 2), as expected for a spherical particle coated with a layer of densely grafted, terminally attached polymer chains. The increase in observed particle diameter was greater than 4 times the radius of gyration of polystyrene of the corresponding molecular weight of the grafted chains, indicating that the chains adopted a stretched conformation from the surface. Consider, for example, the final entry in Table 2. The hydrodynamic diameter of the nanoparticle was 112 nm, and therefore, the average thickness of the polymer layer was 20.5 nm. Two times the radius of gyration, in THF, for polystyrene of $M_n = 1.43 \times 10^4$ is ∼8 nm. Such stretched chains are characteristic for polymer brushes. If significant termination occurred by radical coupling between two chains on different particles, then a large increase in the hydrodynamic diameter versus conversion as well as an increase in the standard deviation of the particle size would have been expected. Together, the GPC and DLS data indicated a minimal occurrence of chain transfer and chain termination during the polymerization.

Thin films of the hybrid nanoparticles were prepared by

(32) Iler, R. K. *The Chemistry of Silica: Solubility, Polymerization, Colloid and Surface Properties, and Biochemistry*; John Wiley and Sons: New York, 1979.

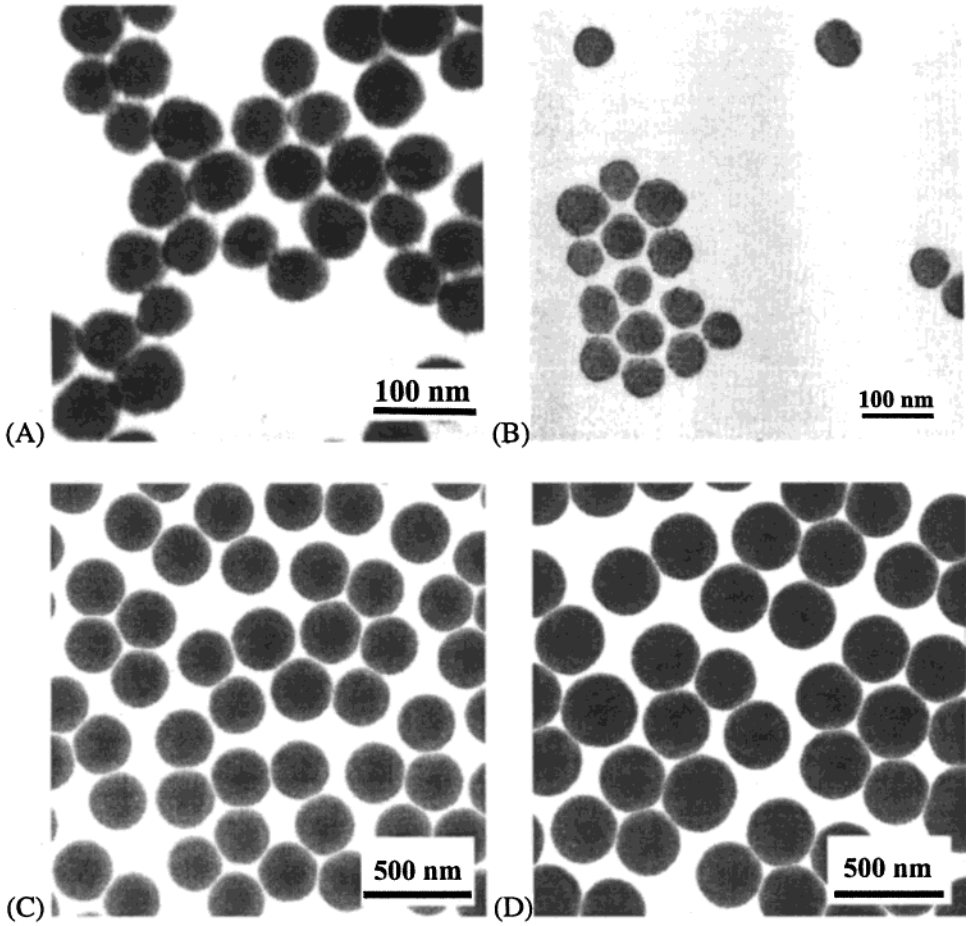

Figure 2. TEM micrographs of (A) BPDS-modified 75-nm SiO_2 nanoparticles, (B) BIDS-modified 75-nm SiO_2 nanoparticles, (C) BPDS-modified 300-nm SiO_2 nanoparticles, and (D) BIDS-modified 300-nm SiO_2 nanoparticles.

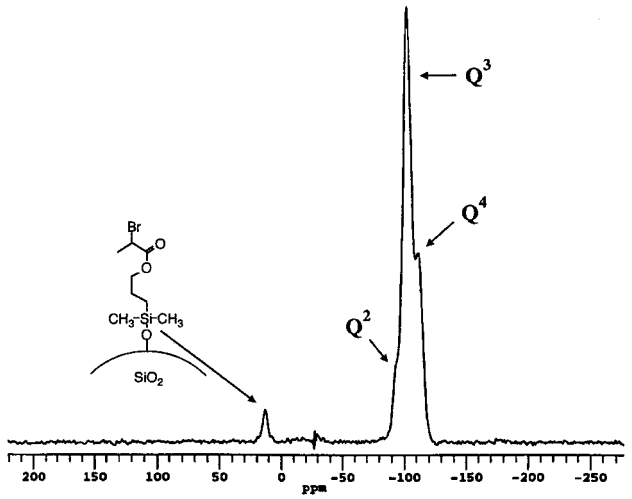

Figure 3. Solid-state ^{29}Si CP-MAS NMR spectrum of BPDS-modified 75-nm-diameter silica nanoparticles showing the chemical shift for the silicon nucleus of the surface-bound initiator at $\delta = 12.2$ ppm.

evaporating a dilute suspension of the particles onto carbon-coated copper grids. TEM micrographs of the composite material showed micrometer-sized polymer film domains containing a monolayer of silica nanoparticles (Figure 5). The silica particles were arranged within the film in a hexagonal array, and the spacing between the particles increased with increasing molecular weight of the grafted polymer. Larger scale ordering was hindered by particle size distribution (~10%) and by incomplete grid coverage. These data demonstrate that it is possible to control the spacing of silica nanoparticles in a polymer film by controlling the molecular weight of the grafted polymer.

Table 1. Characterization Data for the Initiator-Modified Silica Nanoparticles

initiator	particle diam (nm)	mmol of initiator/ g of sample	no. of initiators/ nm^2 of surface
BPDS	75	2.5×10^{-1}	3.7
BPDS	300	7.3×10^{-2}	4.3
BIDS	75	1.7×10^{-1}	2.4
BIDS	300	8.6×10^{-2}	5.0

In contrast to the styrene polymerizations, MMA ATRP from the 75-nm-diameter particles did not exhibit molecular weight control. The kinetic plot shown in Figure 6 showed curvature, and the plot of number-averaged molecular weight versus conversion showed a deviation from a linear correspondence. The molecular weight distributions also increased consistently with conversion up to $M_w/M_n \sim 2.0$. The differences between the ATRP of styrene and MMA from the 75-nm-diameter nanoparticles most likely can be ascribed to differences in the termination mechanism. As shown previously, molecular weight control in ATRP occurs via the persistent radical effect.[33] Initially, a few percent of radical coupling serves to build up a concentration of deactivator (copper(II) species), which in sufficient concentrations will deactivate intermediate radicals faster than the rate at which the radicals can react in termination events. Chain termination is not completely eliminated during the course of the polymerization, though. Some chain termina-

(33) Matyjaszewski, K.; Patten, T. E.; Xia, J. H. *J. Am. Chem. Soc.* **1997**, *119*, 674−680.

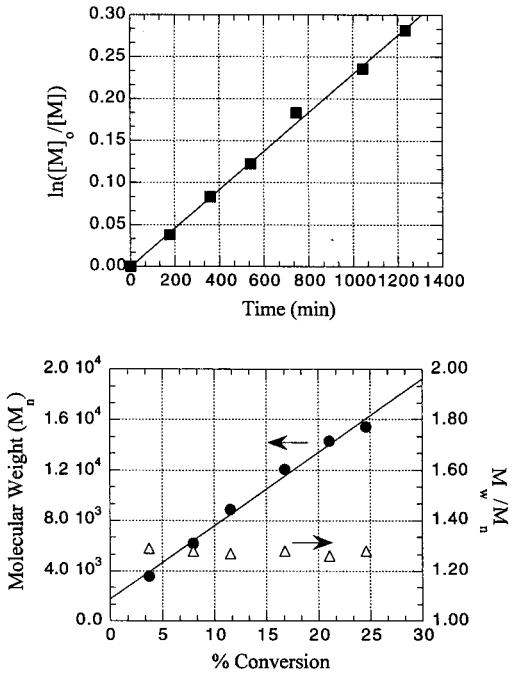

Figure 4. First-order kinetic plot (■) and molecular weight vs conversion plot (●, △) for the ATRP of styrene from the surface of 75-nm BPDS-functionalized silica. Conditions: temperature 110 °C, solvent *p*-xylene, $[\text{styrene}]_0 = 8.73$ M, $[\text{CuBr}]_0 = 61.6$ mM, $[\text{dNbipy}]_0 = 116$ mM, and 1.00 g of SiO_2/initator.

tion will occur at a very slow rate, as seen by the gradual increase in deactivator concentration over time. In a graft polymerization from the surfaces of discreet particles and in the presence of free chains in solution, there are four possible termination modes (Figure 7): termination between free chains in solution, termination between a free chain and a surface-bound chain, termination between chains on the same particle surface, and termination between chains on different particle surfaces. Of these four modes, the rates of termination involving free chains (in solution and to the surface) should be faster than those involving only surface-bound chains (intraparticle and interparticle), because in the former two modes some component can diffuse freely. Of the two modes involving free chains, the rate of termination in solution should be faster than the rate of termination to the surface. The former mode involves two freely diffusing chains while the latter mode has only one freely diffusing component and also incurs an entropic cost by requiring interpenetration of a free chain with the polymer layer about a particle. Evidence for this relative ordering of rates was obtained by Prucker and Ruhe,[9] who demonstrated in the free-radical grafting of polystyrene from silica gel that the molecular weights of the free chains in solution did not change with conversion, while the molecular weight of the surface-bound chains did exhibit some dependence upon conversion. Of the two modes involving surface-bound chains, the rates of termination should both be slow, and without more quantitative data, it is not possible to judge which of the two will be faster. Intraparticle termination has the spatial requirement that two active chains be close to each other on the surface. The probability of this occurrence should be very low, because at any given moment in a controlled radical polymerization less than 1% of the polymer chains will be in the active state. Interparticle termination has the spatial requirement that two particles must collide in orientations such that two active chain ends can meet. This mode also requires interpenetration of the polymer layers on the two particles. Thus, the ordering of the rates of termination should be in solution > to surface > intraparticle ≈ interparticle.

Styrene ATRP is conducted at temperatures at which the rate of thermal polymerization is consequential. Thus, in the styrene polymerizations, some free chains will always be generated in solution, ensuring that any termination that occurs will be predominantly in solution (with some fraction of termination to the surface), that the surface-bound polymer will grow relatively unimpeded, and that the radical concentration will remain constant. MMA does not undergo thermal polymerization, so the predominant termination modes will be interparticle or intraparticle. Additionally, chain termination in the radical polymerization of MMA is predominantly (>90%) via disproportionation.[34] This process would form some macromonomer chain ends that could further react in the polymerization to yield branched and cross-linked structures. Considering the high density of chains on each nanoparticle, even a small amount of such cross-linking would lead to an extensive network. Indeed, when too high a concentration of catalyst was used in the MMA polymerizations, an infusible cross-linked network formed. With lower catalyst concentrations, the polymerizations proceeded; however, a decrease in the rate of polymerization was observed, consistent with chain termination (Figure 6). The deviation observed in the plot of number-averaged molecular weight versus conversion and the high polydispersities (up to 2.0) were both consistent with the aforementioned cross-linking/branching process.

The styrene ATRP system indicated that the molecular weight control in MMA ATRP from 75-nm-diameter nanoparticles should be improved if free chains are present in the polymerization solution. Figure 8 shows the polymerization data for the same MMA polymerization as in Figure 6, except that the free initiator, ethyl 2-bromoisobutyrate, was added. Better molecular weight control was observed in that the kinetic plot shown in Figure 8 showed much less curvature than in Figure 6, and the plot of number-averaged molecular weight versus conversion was essentially linear within the error of the experiment. Each polymer sample comprising the data points had a narrow molecular weight distribution ($M_w/M_n < 1.25$). DLS experiments yielded similar results as for the polymerization of styrene from the 75-nm particles. The hydrodynamic diameter of the composite nanoparticle increased with the molecular weight of the pendant polymer (Table 3), corresponding to the growth of a layer of densely grafted, terminally attached polymer chains.

The polymerizations of styrene and MMA from the 300-nm particles clearly did not exhibit characteristics of a controlled/"living" polymerization. The kinetic plots, as seen for styrene in Figure 9, exhibited deceleration curvature, and the number-average molecular weight versus conversion plots showed deviations from the expected linear correlation. Additionally, the molecular weight distributions of the polymer samples comprising the data points increased as a function of conversion (up to $M_w/M_n = 1.6$).

The contrast in polymerization behavior between polymerizations employing smaller versus larger initiator-modified nanoparticles can be correlated with the amount of initiator present per unit mass of initiator. The 75-nm-diameter particles contain approximately 0.1−0.3 mmol of initiator sites per gram of silica, so a polymerization with 1 g of sample in a 65% solution of monomer yields initial monomer-to-initiator ratios ($[M]_o/[I]_o$) of 200−300. These initiator concentrations and $[M]_o/[I]_o$'s are typical for ATRP experiments that exhibit good molecular

(34) Zammit, M. D.; Davis, T. P.; Haddleton, D. M.; Suddaby, K. G. *Macromolecules* **1997**, *30*, 1915−1920.

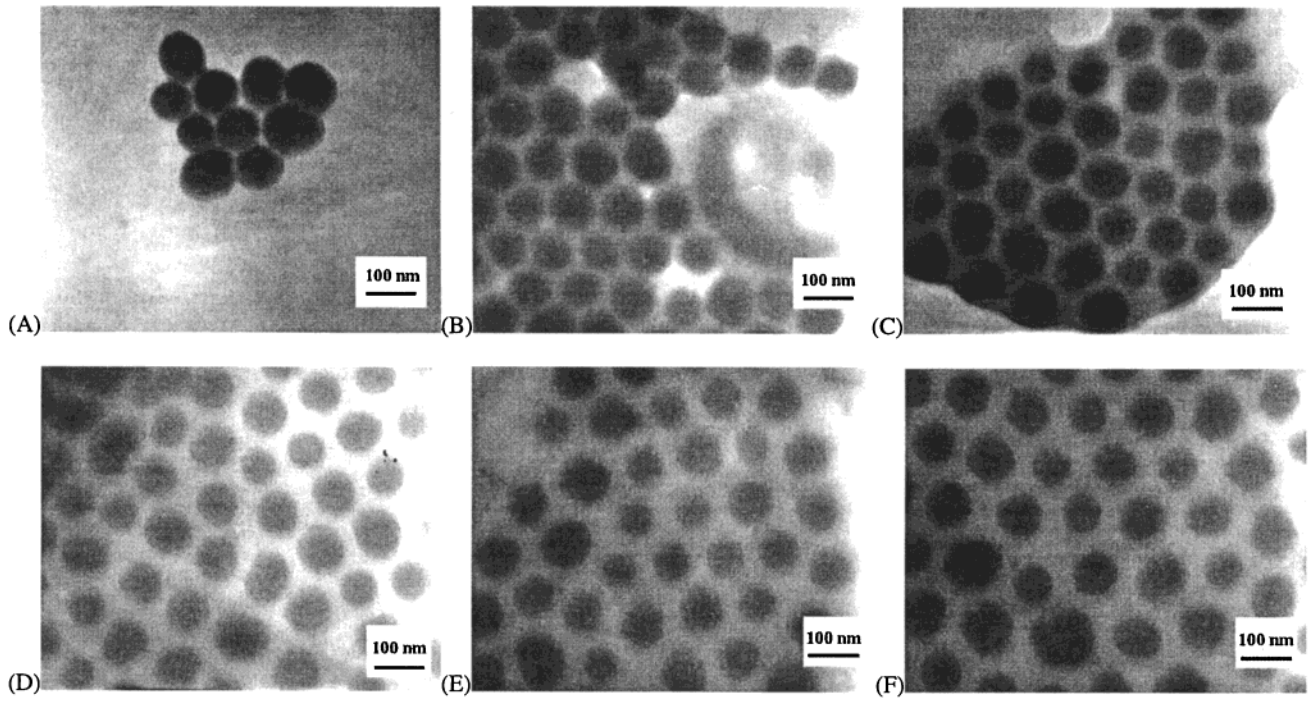

Figure 5. TEMs vs conversion for the data shown in Figure 4 and Table 2. Percent conversions: (A) 3.7, (B) 7.9, (C) 11.6, (D) 16.7, (E) 21.0, and (F) 24.6.

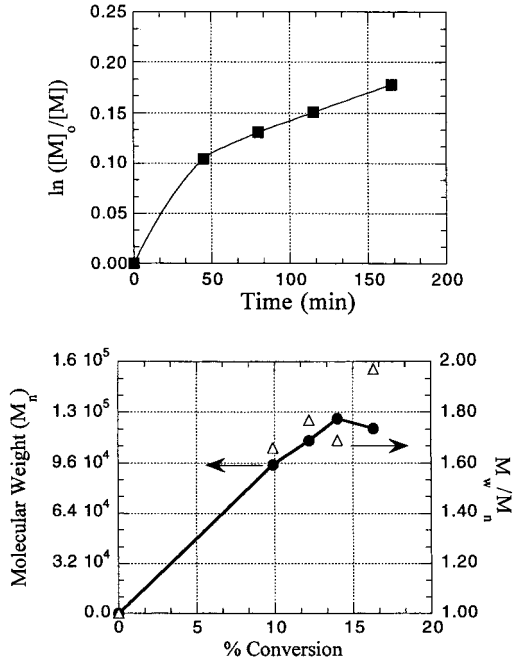

Figure 6. First-order kinetic plot (■) and molecular weight vs conversion plot (●, △) for the ATRP of MMA from the surface of 75-nm BIDS-functionalized silica. Conditions: temperature 90 °C, solvent *p*-xylene, $[MMA]_0 = 4.67$ M, $[CuBr]_0 = 25.2$ mM, $[dNbipy]_0 = 48.7$ mM, and 1.00 g of SiO_2/initator.

weight control. In contrast, the 300-nm-diameter particles contain approximately 0.07−0.09 mmol of initiator sites per gram of silica. The corresponding $[M]_0/[I]_0$ for a polymerization using 1 g of sample in a 65% solution of monomer is 3−4 times greater (approximately 500−800). As shown above, it appears that only 25% of the initiator present on the nanoparticle surface can initiate the growth of chains, so the real $[M]_0/[I]_0$'s for the latter polymerization systems are likely well beyond the upper limit for good molecular weight control in ATRP.

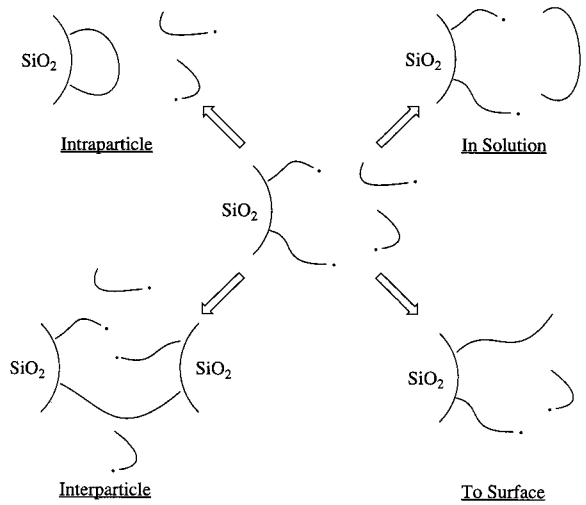

Figure 7. Scheme of the possible termination modes for the ATRP of vinyl monomers from nanoparticle surfaces.

Previous studies showed that the necessary concentration of copper(II) species to ensure a fast rate of radical deactivation was on the order of $10^{-3}-10^{-4}$ M.[35] In polymerizations using the 300-nm-diameter nanoparticles, the concentration of initiator sites for 1 g of initiator-modified nanoparticles in 5-mL total volume of a polymerization was $\sim 10^{-4}$ M. Thus, a sufficient concentration of deactivator could never be generated in the polymerization, and consequently, the rate of radical deactivation was slow. Thus, many monomer additions occurred per activation/deactivation cycle (i.e., uncontrolled chain growth), and a significant amount of termination likely occurred. In the case of the 75-nm-diameter nanoparticles, the concentration of initiator sites for 1 g of silica in 5-mL total volume of a polymerization was on the order of 10^{-3} M. Thus, in these polymerizations, it is possible to build up the requisite copper-

(35) Matyjaszewski, K.; Kajiwara, A. *Macromolecules* **1998**, *31*, 548−550.

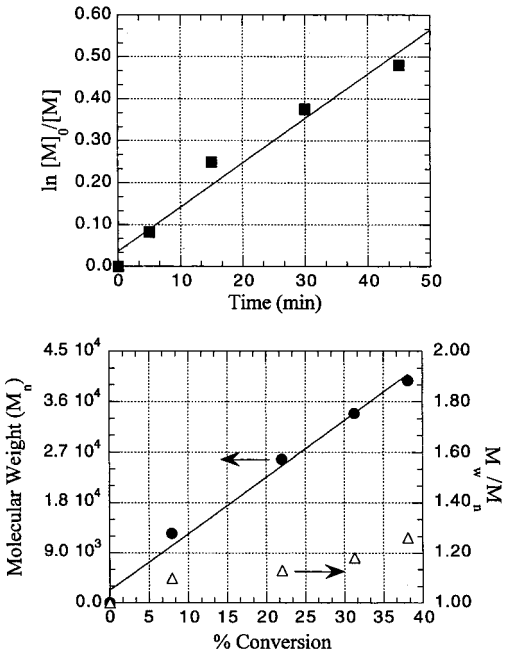

Figure 8. First-order kinetic plot (■) and molecular weight vs conversion plot (●, △) for the ATRP of MMA with added free initiator from the surface of 75-nm BIDS-functionalized silica. Conditions: temperature 90 °C, solvent *p*-xylene, $[MMA]_0 = 4.67$ M, $[CuBr]_0 = 25.1$ mM, $[dNbipy]_0 = 48.8$ mM, [ethyl 2-bromoisobutyrate]$_0 = 4.09$ mM, and 1.00 g of SiO_2/initator.

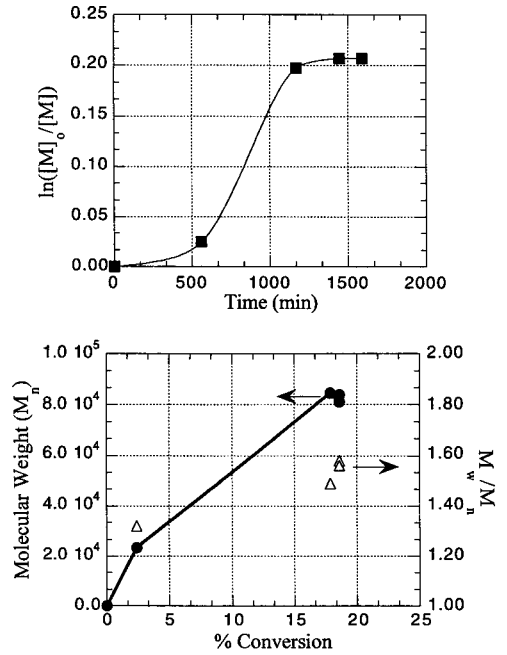

Figure 9. First-order kinetic plot (■) and molecular weight vs conversion plot (●, △) for the ATRP of styrene from 300-nm BPDS-functionalized silica. Conditions: temperature 110 °C, solvent *p*-xylene, $[styrene]_0 = 5.81$ M, $[CuBr]_0 = 37.5$ mM, $[dNbipy]_0 = 74.8$ mM, and 1.00 g of SiO_2/initator.

(II) concentration to ensure a fast rate of deactivation and controlled chain growth.

As discussed above, the polymerizations of MMA and styrene from the 300-nm-diameter nanoparticles did not exhibit molecular weight control. These results were similar to observations made in studies of ATRP initiated from flat surfaces.[15,18] Those studies used ellipsometry, an indirect method for probing chain growth, because the total amount of grafted polymer was too

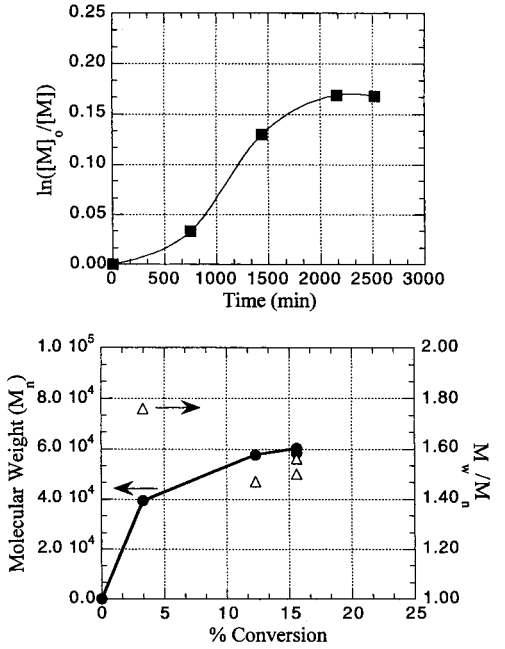

Figure 10. First-order kinetic plot (■) and molecular weight vs conversion plot (●, △) for the ATRP of styrene with added Cu(II) from 300-nm BPDS-functionalized silica. Conditions: temperature 110 °C, solvent *p*-xylene, $[styrene]_0 = 7.04$ M, $[CuBr]_0 = 37.6$ mM, $[dNbipy]_0 = 76.1$ mM, $[CuBr_2/dNbipy]_0 = 2.5$ mM, and 1.00 g of SiO_2/initator.

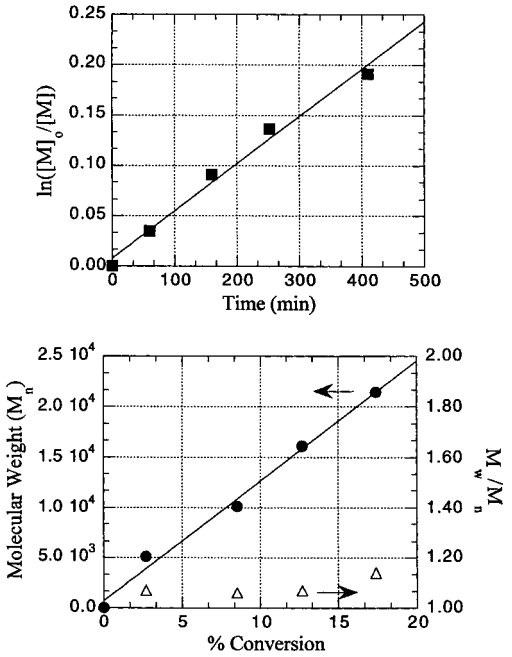

Figure 11. First-order kinetic plot (■) and molecular weight vs conversion plot (●, △) for the ATRP of styrene with added free initiator from 300-nm BPDS-functionalized silica. Conditions: temperature 110 °C, solvent *p*-xylene, $[styrene]_0 = 7.04$ M, $[CuBr]_0 = 37.5$ mM, $[dNbipy]_0 = 74.8$ mM, [ethyl 2-bromopropionate]$_0 = 6.16$ mM, and 1.00 g of SiO_2/initator.

small for isolation and analysis. Recently, though, Kim and coworkers[36] reported a direct measurement of the molecular weight of PMMA grafted from a gold surface using ATRP. Reports have indicated that molecular weight control in surface-initiated ATRP can be induced by either adding free initiator[15] or a deactivator copper(II) complex[18] to the initial polymerization

(36) Kim, J.-B.; Bruening, M. L.; Baker, G. L. *J. Am. Chem. Soc.* **2000**, *122*, 7616−7617.

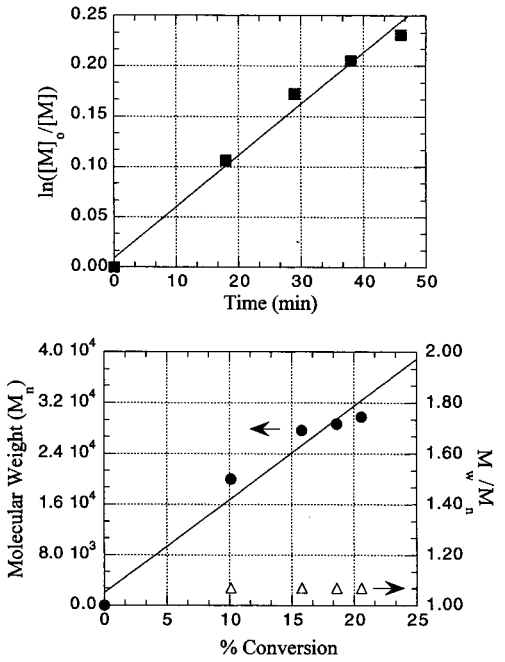

Figure 12. First-order kinetic plot (■) and molecular weight vs conversion plot (●, △) for the ATRP of MMA with added free initiator from the surface of 300-nm BIDS-functionalized silica. Conditions: temperature 90 °C, solvent *p*-xylene, $[MMA]_0 = 4.67$ M, $[CuBr]_0 = 7.25$ mM, $[dNbipy]_0 = 14.7$ mM, [ethyl 2-bromoisobutyrate]$_0 = 4.09$ mM, and 2.03 g of SiO_2/initator.

Table 2. Molecular Weight and DLS Data for the Polymerization of Styrene with BPDS−Modified Silica Nanoparticles (Corresponding to Figure 5)

% conversion	hydrodynamic diam, nm (Std Dev)	M_n of grafted polymer	M_w/M_n of grafted polymer
0	71 (3.7)		
3.7	77 (4.9)	3.60×10^3	1.29
7.9	88 (5.7)	6.20×10^3	1.28
11.6	92 (4.5)	8.90×10^3	1.27
16.7	105 (5.0)	1.20×10^4	1.28
21.0	112 (5.2)	1.43×10^4	1.26
24.6		1.54×10^4	1.28

Table 3. Molecular Weight and DLS Data for the Polymerization of MMA with BIDS-Modified Silica Nanoparticles and Added Free Initiator (Corresponding to Figure 8)

% conversion	hydrodynamic diam, nm (Std Dev)	M_n of grafted polymer	M_w/M_n of grafted polymer
0	69 (2.9)		
7.9	75 (7.4)	1.25×10^4	1.10
22.0	105 (5.8)	2.57×10^4	1.13
31.3	115 (3.5)	3.39×10^4	1.18
38.1	129 (4.3)	3.98×10^4	1.26

solution. The effects of adding free initiator to the polymerization mixture were discussed above. The addition of a copper(II) complex provides a sufficient deactivator concentration in polymerizations where the initial concentration of initiator and copper(I) catalyst are low, and the additional copper(II) complex also mitigates the need for radical coupling to build up the deactivator concentration. We examined the efficacy of these methods in controlling MMA and styrene polymerizations from the 300-nm-diameter nanoparticle surfaces.

First, we repeated the styrene and MMA polymerizations from the 300-nm silica particles except that 5 and 15 mol % of the complex, 2dNbipy/$CuBr_2$, were added to the initial polymerization solutions, respectively. The addition of deactivator slowed the rates of both polymerizations considerably, but little improvement was observed in the plots of molecular weight and molecular weight distribution versus conversion (Figure 10). At first, these results might appear contradictory to those reported previously for ATRP from flat substrates.[18] However, if one interpolates the data at shorter time scales, as used in the previous study (i.e., 1000 min or less), one will see that the number-average molecular weight of the grafted polymer should increase with conversion in that region. Thus, on a flat substrate one might observe an increase in film thickness as a function of time.

Table 4. GPC Data for the Free and Surface-Bound Polymer Chains from the Surface-initiated ATRP of Styrene and MMA with Added Free Initiator (300-nm-diameter silica particles)

	free polymer in solution		surface-grafted polymer	
monomer	mol wt (M_n)	M_w/M_n	mol wt (M_n)	M_w/M_n
styrene[a]	4.38×10^4	1.22	4.63×10^4	1.29
MMA[b]	5.07×10^4	1.16	4.31×10^4	1.26

[a] Three times the quantities used for the polymerization described in Figure 11. Final conversion, 35%. [b] Two times the quantities used for the polymerization described in Figure 12. Final conversion, 41%.

Next, we repeated the styrene and MMA polymerizations from the 300-nm silica particles, except that 60 mol % of ethyl 2-bromopropionate (styrene) or 50 mol % of ethyl 2-bromoisobutryate (MMA) was added to the initial polymerization solution. The ATRP of both styrene and MMA in the presence of added free initiator displayed the elements of a controlled polymerization (Figures 11 and 12, respectively). The first-order kinetic plots showed essentially a linear relationship between $\ln([M]_o/[M])$ and time within the error of the experiment, and also the plots of number-average molecular weight versus conversion were essentially linear. Each sample comprising the data points had a narrow molecular weight distribution (1.07−1.20), and the GPC traces showed Gaussian distributions. The molecular weight distributions indicated that even though polymerization occurred both in solution and from the surface, all the polymer chains all grew at the same rate. Additional support for this conclusion was gained by separating the surface-grafted polymer from the free polymer. The polymerizations were repeated using 3 (styrene) or 2 (MMA) times the quantities used for the polymerizations in Figures 11 and 12, respectively, and the kinetics and evolution of molecular weights versus conversion were monitored to check that the polymerization still exhibited good molecular weight control. We centrifuged the final polymerization mixtures and decanted the supernatant. Fresh THF was added, and this process was repeated until a precipitate did not form when the supernatant was added to methanol. The free polymer was isolated from the collective supernatants by precipitation, and the surface-grafted polymer was isolated by etching the silica cores with HF followed by precipitation. Both sets of samples were analyzed using GPC, and the results are shown in Table 4. For the polymerizations of both styrene and MMA, there was essentially little difference, within experimental error, between the molecular weights and molecular weight distributions of the free and surface-bound polymer chains. The molecular weight distributions were slightly higher for the surface-grafted chains when compared to the free chains, a feature of surface-initiated ATRP that was predicted by Matyjaszewski and co-workers.[18] These sets of molecular weight distributions suggest that the rate of exchange between active and dormant chain ends in solution and bound to the nanoparticle surface was sufficiently fast that (1) all chains grew

at the same rate and (2) the collective molecular weight data shown in Figures 11 and 12 can be considered reflective of the growth of polymer chains from the surface.

The experimental data indicated that the growth of polymer chains from the 300-nm-diameter particles exhibited all the characteristics of a controlled/"living" polymerization when free initiator was present. A key difference between the polymerizations with added Cu(II) and added free initiator was that the latter polymerizations had a lower initial monomer-to-initiator ratios, thus allowing for better molecular weight control. It was not possible to conduct a polymerization using the 300-nm silica particles and added Cu(II) that had the same initial monomer-to-initiator ratios used in the polymerizations with added free initiator. Such polymerizations would have required concentrations of more than 1 g/mL of initiator-modified silica in bulk monomer. Thus, a direct comparison of the two systems was not possible.

However, it was possible to test whether the larger initial monomer-to-initiator ratios were a sufficient condition for observing worse molecular weight control. The ATRP of styrene using BPDS-modified 75-nm silica was repeated using the same conditions as in Figure 4 except that the concentrations of Cu(I) and initiator were halved. The polymerization no longer exhibited the characteristics of a controlled radical polymerization. The molecular weights did not increase with monomer conversion after 10% conversion, and the molecular weight distributions were large (up to 1.50). The polymerization showed behavior similar to that observed with the 300-nm particles, indicating that very high monomer-to-initiator ratios are problematic in conducting a controlled polymerization from nanoparticle surfaces.

In the spectrum of polymerization substrates, the 75-nm-diameter nanoparticles resemble small molecule initiators in their polymerization behavior. The 300-nm-diameter nanoparticles, with their small quantities of initiation sites, more closely resemble flat substrates and could be used as models. Silica gel has been used as a model for polymerizations from flat surfaces; however, it has a high surface area ($\sim 10^2$ m^2 g^{-1}). A silica surface has an average hydroxyl group content of 2.5−5.0 mmol g^{-1}, so the resulting initiator-modified silica gel would have initiator contents $\sim$1 order of magnitude higher than that of the 75-nm-diameter silica nanoparticles and therefore even higher than that of a flat silica surface. An important feature of the 300-nm-diameter nanoparticles is that while they model the kinetic and molecular weight evolution behavior of initiator-modified flat surfaces, the initiator content is still sufficiently high that the grafted polymer can be cleaved from the particles and isolated. Consequently, the molecular weights and molecular weight distributions can be analyzed, and the polymerization chemistry can be probed in detail. The 300-nm-diameter nanoparticles, therefore, could serve as models for surface-initiated polymerizations from flat substrates.

Conclusions

Structurally well-defined polymer−nanoparticle hybrids were prepared by modifying the surface of silica nanoparticles with initiators for ATRP and by using these initiator-modified nanoparticles as macroinitiators. Polymerizations of styrene and MMA using the nanoparticle initiators displayed the diagnostic criteria for a controlled/"living" radical polymerization under specific reaction conditions. Well-defined polymer chains were grown from the nanoparticle surfaces to yield individual particles composed of a silica core and a well-defined, densely grafted outer polystyrene or poly(methyl methacrylate) layer. Polymerizations of styrene from smaller (75-nm-diameter) silica nanoparticles exhibited good molecular weight control, while polymerizations of MMA from the same nanoparticles exhibited good molecular weight control only when a small amount of free initiator was added to the polymerization solution. The polymerizations of both styrene and MMA from larger (300-nm-diameter) silica nanoparticles did not exhibit molecular weight control. Molecular weight control was induced by the addition of a small amount of free initiator to the polymerization but was not induced when 5−15 mol % of deactivator (Cu(II) complex) was added. These findings provide guidance for future efforts in using ATRP for the controlled grafting of polymers from high surface area substrates (i.e., small-diameter cylinders and spheres, highly porous materials) and low surface area substrates (i.e., flat surfaces, large-diameter cylinders and spheres, low-porosity materials).

Acknowledgment. This work was supported by the NSF CAREER program (DMR-9733786).

Supporting Information Available: The experimental section; DRIFT spectrum of BPDS-modified 75-nm-diameter silica nanoparticles; IR spectra for the etching of the polystyrene and PMMA-grafted nanoparticles with HF; first-order kinetic plots and molecular weight vs conversion plots for (1) the ATRP of MMA from the surface of 300-nm-diameter BIDS functionalized silica, (2) the ATRP of MMA from the surface of 300-nm-diameter BIDS functionalized silica with added Cu(II), and (3) the ATRP of styrene from the surface of 75-nm BPDS-functionalized silica under high initial monomer-to-initiator ratio conditions. This material is available free of charge via the Internet at http://pubs.acs.org. See any current masthead page for ordering information and Web access instructions.

JA010235Q